

Supporting Information

Mechanism of Roughness-induced CO₂ Microbubble Nucleation in Polypropylene Foaming

Linyan Wang^{a,c}, Wei Zhang^c, Xiangdong Wang^{a,*}, Jianguo Mi^b, Jingjun Ma^c, and Zhongjie Du^{b,*}

^a School of Materials and Mechanical Engineering, Beijing Technology and Business University, Beijing, China

^b The Key Laboratory of Carbon Fiber and Functional Polymers, Ministry of Education, Beijing University of Chemical Technology, Beijing, China

^c Institute of Technology in Bohai Campus, Agricultural University of Hebei, China

1. Calculation of Helmholtz free energy

The fundamental measure theory is commonly used to describe the contribution of hard-sphere repulsion,¹ which is expressed as

$$F^{\text{hs}}[\{\rho_\alpha(\mathbf{r})\}] = k_B T \int \Phi^{\text{hs}}[n_\gamma(\mathbf{r})] d\mathbf{r} \quad (\text{S1})$$

where the detail information $\Phi^{\text{hs}}[n_\gamma(\mathbf{r})]$ can be seen elsewhere.²

With the weighted density approximation, the attractive part can be expressed as³

$$F^{\text{att}}[\{\rho_\alpha(\mathbf{r})\}] = k_B T \sum_\alpha \int (\rho_\alpha(\mathbf{r}) \{F_1[\bar{\rho}_\alpha(\mathbf{r})] + F_2[\bar{\rho}_\alpha(\mathbf{r})]\}) d\mathbf{r}, \quad (\text{S2})$$

* Corresponding authors: wangxid@th.btbu.edu.cn; duzj@mail.buct.edu.cn

in which the expressions of $F_1[\bar{\rho}_\alpha(\mathbf{r})]$ and $F_2[\bar{\rho}_\alpha(\mathbf{r})]$ are given by the first-order mean spherical approximation expansion

$$\begin{aligned}
F_1[\bar{\rho}_\alpha(\mathbf{r})] = & -2\pi\bar{\rho}_\alpha(\mathbf{r})\beta\sum_\alpha\sum_{\alpha'}x_\alpha x_{\alpha'}\varepsilon_{\alpha\alpha'}\left[k_{1,\alpha\alpha'}\left(G_{0,\alpha\alpha'}(z_{1,\alpha\alpha'})e^{\bar{z}_{1,\alpha\alpha'}R_{\alpha\alpha'}}-\frac{1+z_{1,\alpha\alpha'}R_{\alpha\alpha'}}{z_{1,\alpha\alpha'}^2}\right)\right. \\
& \left.-k_{2,\alpha\alpha'}\left(G_{0,\alpha\alpha'}(z_{2,\alpha\alpha'})e^{\bar{z}_{2,\alpha\alpha'}R_{\alpha\alpha'}}-\frac{1+z_{2,\alpha\alpha'}R_{\alpha\alpha'}}{z_{2,\alpha\alpha'}^2}\right)\right]+8\pi\bar{\rho}_\alpha(\mathbf{r})\beta\sum_\alpha\sum_{\alpha'}x_\alpha x_{\alpha'}\varepsilon_{\alpha\alpha'}R_{\alpha\alpha'}^3I_{\alpha\alpha',\infty} \\
& -8\pi\bar{\rho}_\alpha(\mathbf{r})\beta\sum_\alpha\sum_{\alpha'}x_\alpha x_{\alpha'}\varepsilon_{\alpha\alpha'}g_{0,\alpha\alpha'}(R_{\alpha\alpha'})R_{\alpha\alpha'}^3I_{\alpha\alpha',1}
\end{aligned} \tag{S3}$$

$$\begin{aligned}
F_2[\bar{\rho}_\alpha(\mathbf{r})] = & -\pi\bar{\rho}_\alpha(\mathbf{r})\beta\sum_\alpha\sum_{\alpha'}x_\alpha x_{\alpha'}\varepsilon_{\alpha\alpha'}\left[k_{1,\alpha\alpha'}\left(G_{1,\alpha\alpha'}(z_{1,\alpha\alpha'})e^{\bar{z}_{1,\alpha\alpha'}R_{\alpha\alpha'}}\right)-k_{2,\alpha\alpha'}\left(G_{2,\alpha\alpha'}(z_{2,\alpha\alpha'})e^{\bar{z}_{2,\alpha\alpha'}R_{\alpha\alpha'}}\right)\right] \\
& -4\pi\bar{\rho}_\alpha(\mathbf{r})\beta\sum_\alpha\sum_{\alpha'}x_\alpha x_{\alpha'}\varepsilon_{\alpha\alpha'}g_{1,\alpha\alpha'}(R_{\alpha\alpha'})R_{\alpha\alpha'}^3I_{\alpha\alpha',1}
\end{aligned} \tag{S4}$$

The weighted density $\bar{\rho}_\alpha(\mathbf{r})$ is defined as

$$\bar{\rho}_\alpha(\mathbf{r}) = \sum_{\alpha'} \int \rho_{\alpha'}(\mathbf{r}') \omega_{\alpha\alpha'}^{\text{att}}(|\mathbf{r}-\mathbf{r}'|) d\mathbf{r}', \tag{S5}$$

where $\omega_{ij}^{\text{att}}(\mathbf{r})$ is the weight function $\omega_{\alpha\alpha'}^{\text{att}}(\mathbf{r}) = u_{\alpha\alpha'}^{\text{att}}(\mathbf{r}) / \int u_{\alpha\alpha'}^{\text{att}}(\mathbf{r}) d\mathbf{r}$, and $u_{\alpha\alpha'}^{\text{att}}(\mathbf{r})$ is the LJ attractive interaction potential between any two sites of species α and α' .

The free energy contribution from the molecular connectivity are based on the associating theory⁴

$$F^{\text{chain}}[\{\rho_\alpha(\mathbf{r})\}] = \int d\mathbf{r}_1 \sum_{\alpha=1}^{N_{\text{site}}} \rho_\alpha^{\text{site}}(\mathbf{r}_1) \times \sum_{\mathbf{a} \in \Gamma^\alpha} \left(\ln X_{\mathbf{a}}^\alpha(\mathbf{r}_1) - \frac{X_{\mathbf{a}}^\alpha(\mathbf{r}_1)}{2} + \frac{1}{2} \right), \tag{S6}$$

where Γ^α means the set of all the associating points on site α , $X_{\mathbf{a}}^\alpha$ corresponds to the fraction of site α which are not bonded at point \mathbf{a} , and N_{site} indicates the total site number of a polymer chain. The first summation of N_{site} is over all the site α , and the second is over all the association points on site α .

The free energy functional due to the contribution of chain conformation is constructed to account for the polymer configurationally entropy

$$F^{\text{conf}}[\{\rho_\alpha(\mathbf{r})\}] = -\frac{1}{2} \sum_\alpha \sum_{\alpha'} \int d\mathbf{r}' \int d\mathbf{r}'' \rho_\alpha(\mathbf{r}') \rho_{\alpha'}(\mathbf{r}'') e_{\alpha\alpha'}^{\text{conf}}(|\mathbf{r}'-\mathbf{r}''|) \tag{S7}$$

with the approximation $c^{\text{conf}}(r) = c^{\text{semiflexible}}(r) - c^{\text{flexible}}(r)$. Here $c^{\text{semiflexible}}(r)$ and $c^{\text{flexible}}(r)$ stand for the direct correlation functions of semiflexible and flexible PP chains. They are calculated from the polymer reference interaction site model integral equation⁵

$$h(r) = \int d\mathbf{r}' \int d\mathbf{r}'' \omega(|\mathbf{r} - \mathbf{r}'|) c(|\mathbf{r}' - \mathbf{r}''|) [\omega(r'') + \rho h(r'')], \quad (\text{S8})$$

where $h(r)$ is the total correlation function, $\omega(r)$ the intramolecular correlation function. $\omega(r)$ for flexible or semiflexible chains are represented by the Koyama model.^{6,7} The Kovalenko–Hirata approximation⁸ is adopted to solve the equation.

2. The external potential of polymer–fluid and nanoparticle–fluid

The interaction between fluid molecule site α and polymer site p is given by the conventional Lenard–Jones (LJ) potential

$$U_{p\alpha}(\mathbf{r}_{p\alpha}) = 4\varepsilon_{p\alpha} \left[\left(\frac{\sigma_{p\alpha}}{\mathbf{r}_{p\alpha}} \right)^{12} - \left(\frac{\sigma_{p\alpha}}{\mathbf{r}_{p\alpha}} \right)^6 \right] \quad (\text{S9})$$

and $\mathbf{r}_{p\alpha}$ denotes to the locations of the interacting sites. The LJ parameters for unlike sites are calculated using the Lorentz–Berthelot mixing rules. The interaction between fluid molecule site α and F-POSS particle n can be calculated by⁹

$$U_{n\alpha}(\mathbf{r}) = -\varepsilon_{n\alpha} \exp \left[-\frac{\mathbf{r}_{n\alpha} - D_{n\alpha}}{\nu\sigma_{\alpha}} \right] \quad (\text{S10})$$

Where $D_{n\alpha}$ is the mixed diameter of F-POSS particle and fluid molecule, the spatial range parameter ν is material dependent, and its value is 0.5, $\mathbf{r}_{n\alpha}$ represents the center distance between a F-POSS particle and a fluid molecule site.

3. Construction of composite surfaces

The crystalline PP structure is directly constructed using the Material Studio. The amorphous PP structure is constructed using the molecular dynamics (MD) simulation. During the simulation of amorphous PP surface, PP chains are placed in a large periodic box to construct the initial configuration. NPT ensemble is employed to compress the systems of low density to the desired density. The system is equilibrated for at least 6 ns with NVT simulations under one bar pressure. Such equilibrated structure is used as initial configuration for further production run of $(10-20) \times 10^6$ MD steps by NPT simulation. During all simulation runs, a time step of 1.0 fs is used with a multiple time step integrator.¹⁰ Isothermal calculations are carried out with a Nose-Hoover thermostat using a coupling frequency of 0.02 fs^{-1} and the pressure is controlled by a Nose-Hoover barostat.¹¹ The bond lengths are constrained using the SHAKE algorithm.¹² The amorphous or crystalline PP surfaces can be represented by a slice of the constructed system. Afterwards, different nanocomposite surfaces are constructed by distributing F-POSS ($D = 1 \text{ nm}$) randomly on surfaces at given particle coverage ratio. On the other hand, PP chains and F-POSS particles are placed in a large periodic box at given particle volume fraction to construct the final amorphous PP nanocomposite. The coverage ratio is then calculated by the statistic averages of particles on the surfaces with several random cuts.

4. Determination of the energy parameter of PP

The prerequisite of a reasonable force field is that it can well reproduce the chemical potential equilibrium inside and outside of pure PP matrix. The TraPPE-UA bonded and nonbonded parameters appear to well describe the structure of PP chains. When these parameters are applied to calculate phase coexistence curves, however, the results deviate systematically from the experimental data. Thus it is necessary to regulate some parameters depending on those experimental measurements. For simplicity, the intramolecular bonding parameters are supposed to remain invariant, whereas the nonbonded energy parameters are regressed using

the experimental data.¹³ Fig. S1 shows the chemical potential variation with increasing density via the grand canonical transformation¹⁴ using the new energy parameter. After about the tenth transform, the curve is visually flat in the range of transition, and the two singular points at both ends represent equilibrium densities outside and inside the PP matrix. Such parameter is then applied to the CO₂/PP/F-POSS ternary systems without further regulation.

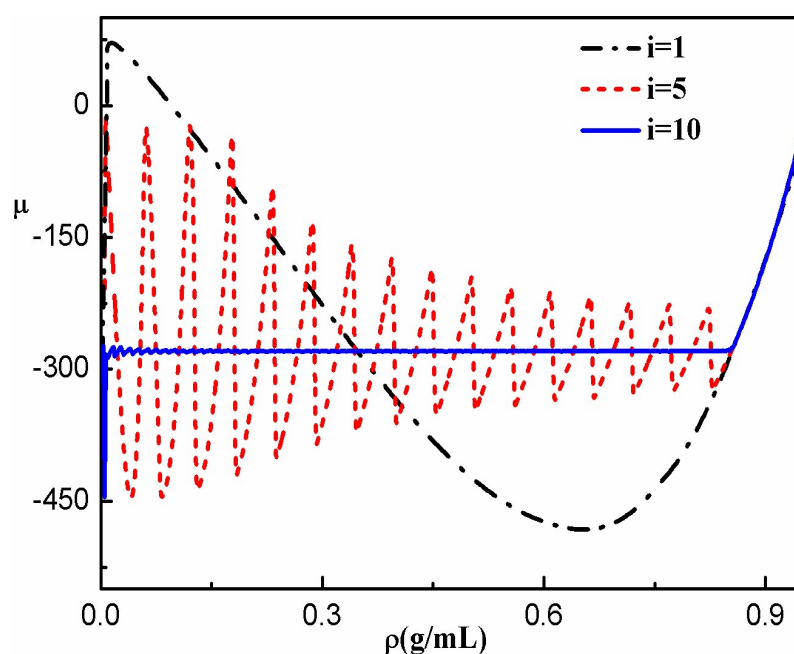


Fig. S1. Transforming process for searching the chemical potential equilibrium outside and inside PP matrix.

5. Solubility

CO₂ solubility plays an important role in PP foaming, and should be addressed in advance. It is generally accepted that crystallites are impenetrable for most non-reactive molecules including CO₂. Small molecules can diffuse into amorphous regions. The crystal domain is usually considered as inert filler because gas cannot access. The CO₂ solubility properties in this work are referring to those in amorphous PP matrix. Fig. S2 presents the experimental and calculated pressure–composition curves for CO₂/PP at different temperatures. The average deviation between calculated and experimental values¹⁵ is 3.70%. At the

beginning of adsorption, the CO₂ composition in PP phase exhibits linear correlation to the pressure. As the pressure increases, CO₂ molecules are forced to penetrate into PP matrix. The influence of temperature on the composition could be explained by its effect on bulk CO₂ density.

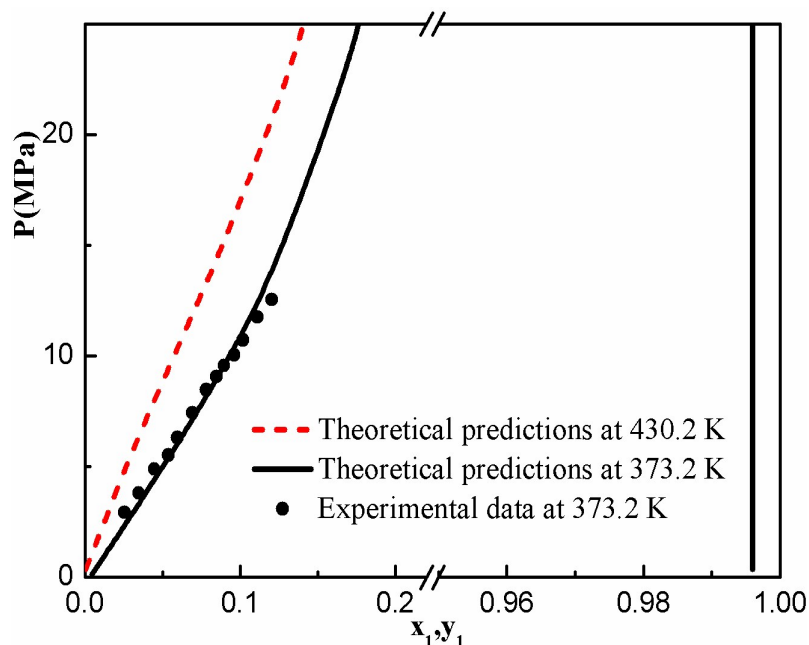


Fig. S2. Pressure–composition curves of CO₂ (1) and PP (2) mixture at different temperatures. x_1 is the mass fraction of CO₂ in PP phase, and y_1 is the mass fraction of CO₂ in CO₂ phase. The spots are experimental data.¹⁵

Fig. S3 illustrates the density variations, where the pressure declines from different initial pressures to the foaming pressure, such as the ambient pressure (0.1MPa). In the process of decompression, CO₂ mass fraction is a constant, but the densities of CO₂ and PP decrease. Nevertheless, the concentration of CO₂ is several orders larger than the equilibrium concentration at the foaming pressure. Therefore, the PP matrix swells, resulting in a further decrease of density and an increase of swelling ratio. In this case, the over-swelled PP matrix provides enough free volume for bubble nucleation and growth. As a consequence, CO₂ concentration shows supersaturation, but the PP concentration declines to subsaturation, which are imperative for the metastable bubble nucleation.

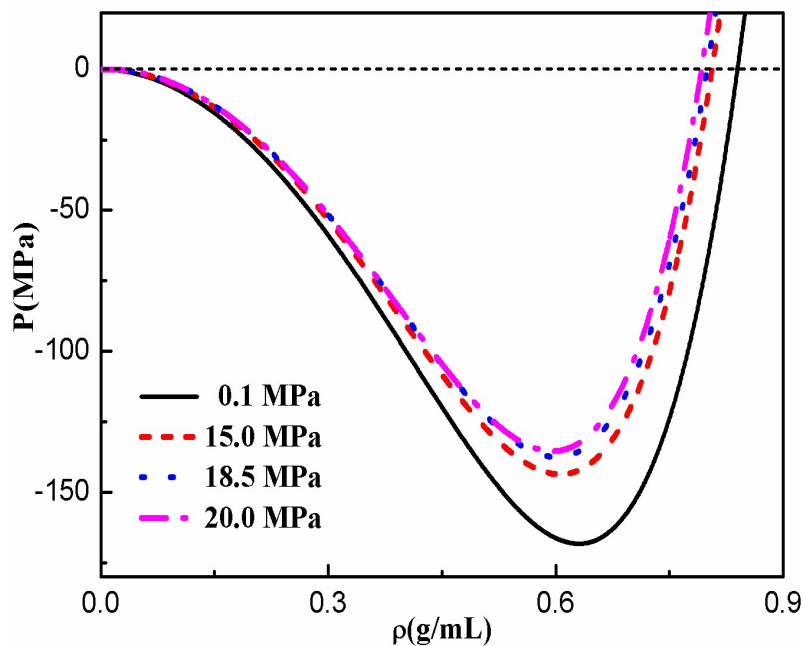


Fig. S3. Pressure–density curves in the systems of CO₂/PP with different mass fractions of CO₂ in PP phase.

The dotted lines switch to the foaming pressure (0.1MPa).

6. Excess free energies

We have calculated the excess free energies for different PP/CO₂ binary systems in contact with the amorphous or crystalline PP surfaces. The results are shown in the following Table S1. It is shown that the contribution of conformational entropy ($\Delta F^{\text{chain}} + \Delta F^{\text{conf}}$) exceeds that of interaction enthalpy ($\Delta F^{\text{hs}} + \Delta F^{\text{att}}$), showing the inherent characteristic of polymer systems. In addition, the interaction of crystal surface exceeds that of amorphous surface at a given particle coverage, resulting in relatively lower surface tension.

Table S1 Excess free energies for the PP/CO₂ binary systems in contact with different composite surfaces.

System	Particle coverage ratio%	ΔF^{id} / $k_{\text{B}}T$	$\Delta F^{\text{hs}} + \Delta F^{\text{att}}$ / $k_{\text{B}}T$	$\Delta F^{\text{chain}} + \Delta F^{\text{conf}}$ / $k_{\text{B}}T$	ΔF^{ext} / $k_{\text{B}}T$
Amorphous	0.00	0.42	0.16	-0.25	-0.092
	42.70	0.039	0.017	-0.023	-
	70.00	0.090	0.036	-0.055	-0.013
Crystalline	0.00	0.39	0.15	-0.22	-0.12
	42.70	0.032	0.014	-0.018	-
	70.00	0.090	0.036	-0.055	-0.013

Notes and references

- 1 Y. Rosenfeld, *Phys. Rev. Lett.*, 1989, **63**, 980.
- 2 Y.-X. Yu and J. Wu, *J. Chem. Phys.*, 2002, **117**, 10156.
- 3 D. Zhou, J. Mi and C. Zhong, *J. Phys. Chem. C*, 2012, **116**, 3042.
- 4 S. Jain, A. Dominik and W. G. Chapman, *J. Chem. Phys.*, 2007, **127**, 244904.
- 5 K. S. Schweizer and J. G. Curro, *Phys. Rev. Lett.*, 1987, **58**, 246.
- 6 K. G. Honnell, J. G. Curro and K. S. Schweizer, *Macromolecules*, 1990, **23**, 3496.
- 7 M. Xu, J. Chen, C. Zhang, Z. Du and J. Mi, *Phys. Chem. Chem. Phys.*, 2011, **13**, 21084.
- 8 A. Kovalenko and F. Hirata, *J. Chem. Phys.*, 1999, **110**, 10095.
- 9 J. B. Hooper and K. S. Schweizer, *Macromolecules*, 2005, **38**, 8858.
- 10 J. G. Curro and A. L. Frischknecht, *Polymer*, 2005, **46**, 6500.
- 11 G. J. Martyna, M. E. Tuckerman, D. J. Tobias and M. L. Klein, *Mol. Phys.*, 1996, **87**, 1117.
- 12 D. Argyris, N. R. Tummala, A. Striolo and D. R. Cole, *J. Phys. Chem. C*, 2008, **112**, 13587.
- 13 J. Li, W. Cheung and D. Jia, *Polymer*, 1999, **40**, 1219.
- 14 Y. Tang, *J. Chem. Phys.*, 2011, **134**, 224508.
- 15 D.-c. Li, T. Liu, L. Zhao and W.-k. Yuan, *Ind. Eng. Chem. Res.*, 2009, **48**, 7117.